Nanomechanics of carbon nanotubes and composites

Deepak Srivastava and Chenyu Wei

Computational Nanotechnology, NASA Ames Research Center, Moffett Field, California 94035-1000; deepak@nas.nasa.gov

Kyeongjae Cho

Department of Mechanical Engineering, Stanford University, Stanford, California 93045

Computer simulation and modeling results for the nanomechanics of carbon nanotubes and carbon nanotube-polyethylene composite materials are described and compared with experimental observations. Young's modulus of individual single-wall nanotubes is found to be in the range of 1 TPa within the elastic limit. At room temperature and experimentally realizable strain rates, the tubes typically yield at about 5–10% axial strain; bending and torsional stiffness and different mechanisms of plastic yielding of individual single-wall nanotubes are discussed in detail. For nanotube-polyethylene composites, we find that thermal expansion and diffusion coefficients increase significantly, over their bulk polyethylene values, above glass transition temperature, and Young's modulus of the composite is found to increase through van der Waals interaction. This review article cites 54 references. [DOI: 10.1115/1.1538625]

1 INTRODUCTION

Since the discovery of multi-wall carbon nanotubes in 1991 by Iijima [1], and subsequent synthesis of single-wall carbon nanotubes by others [2,3] there are numerous experimental and theoretical studies of their electronic, chemical, and mechanical properties. Chemical stability, diverse electronic properties (ranging from 1eV band gap semiconductors to metals), and predicted extreme strength of the nanotubes have placed them as fundamental building blocks in the rapidly growing field of nanotechnology. Diverse nanoscale device concepts have been proposed to develop nanoscale electronic devices, chemical sensors, and also high strength nanotube composite materials with sensing and actuating capacity. To realize the proposed devices and materials concepts, it is crucial to gain detailed understanding on the fundamental limits of nanotubes' diverse properties. Atomistic simulations are a very promising approach to achieve this goal since one can investigate a large range of possibilities which are often very difficult to access through experimental studies. The insights and detailed mechanistic understanding provide valuable guiding principles to optimize and develop novel nanoscale devices and materials concepts.

In this review article, we focus our discussion on the mechanical properties of carbon nanotubes in the context of high-strength nanotube composite materials. For this purpose, it is crucial to gain a detailed understanding of the nanotubes' intrinsic mechanical properties, as well as their interaction with the polymer matrix in nanotube-polymer composite materials. First, we will examine the elastic and failure properties of nanotubes to understand their fundamental strength and stiffness behavior. Initial atomistic simulations of nanotube mechanics have predicted unusually large Young's moduli (of up to 5TPa or 5 times larger than the modulus of diamond) and elastic limits (of up to 20–30% strain before failure). These predictions immediately raised the intriguing possibility of applying the nanotubes as super strong reinforcing fibers with orders of magnitude higher strength and stiffness than any other known material. Subsequently, more accurate simulations employing tight-binding molecular dynamics methods and *ab-initio* density functional total energy calculations involving realistic strain rate, temperature dependence, and nanotube sizes have provided more realistic values of 1TPa as Young's modulus and 5–10% elastic limit of the strain before failure. These values predict 50 GPa as the nanotube strength, in good agreement with recent experimental observations. Second, we will examine the mechanical properties of nanotube-polymer composite materials to understand the mechanisms of mechanical load transfer between a polymer matrix and embedded nanotubes. This research area is rapidly moving forward with exciting possibilities of designing and developing very small structures (eg, MEMS devices) with tailored mechanical properties. Near-term practical applications of nanotubes are expected to emerge from the composite materials, as they do not require a precise control of nanotube positioning for device applications. For the future development of smart nanotube-polymer composite materials, computational mod-

Transmitted by Associate Editor AK Noor

eling will play a catalytic role in facilitating and accelerating the design and fabrication of composite materials with sensing, actuation, and self-healing capabilities.

2 CARBON NANOTUBES: STRUCTURE AND PROPERTIES

A single-wall carbon nanotube (SWNT) is best described as a rolled-up tubular shell of graphene sheet [Fig. 1*a*] [4,5]. The body of the tubular shell is mainly made of hexagonal rings (in a sheet) of carbon atoms, where as the ends are capped by a dome-shaped half-fullerene molecules. The natural curvature in the sidewalls is due to the rolling of the sheet into the tubular structure, whereas the curvature in the end caps is due to the presence of topological (pentagonal ring) defects in the otherwise hexagonal structure of the underlying lattice. The role of the pentagonal ring defect is to give a positive (convex) curvature to the surface, which helps in closing of the tube at the two ends. A multi-wall nanotube (MWNT) is a rolled-up stack of graphene sheets into concentric SWNTs, with the ends again either capped by half-fullerenes or kept open. A nomenclature (n,m) used to identify each single-wall nanotube, in the literature, refers to integer indices of two graphene unit lattice vectors corresponding to the chiral vector of a nanotube [4]. Chiral vectors determine the directions along which the graphene sheets are rolled to form tubular shell structures and perpendicular to the tube axis vectors, as explained in Ref. [4]. The nanotubes of type (n, n), as shown in Fig. 1*b*, are commonly called armchair nanotubes because of the _/‾_/ shape, perpendicular to the tube axis, and have a symmetry along the axis with a short unit cell (0.25 nm) that can be repeated to make the entire section of a long nanotube. Other nanotubes of type (n, 0) are known as zigzag nanotubes (Fig. 1*c*) because of the /\/\/ shape perpendicular to the axis, and also have a short unit cell (0.43 nm) along the axis. All the remaining nanotubes are known as chiral or helical nanotubes and have longer unit cell sizes along the tube axis. Details of the symmetry properties of the nanotubes of different chiralities are explained in detail in Refs. [4] and [5].

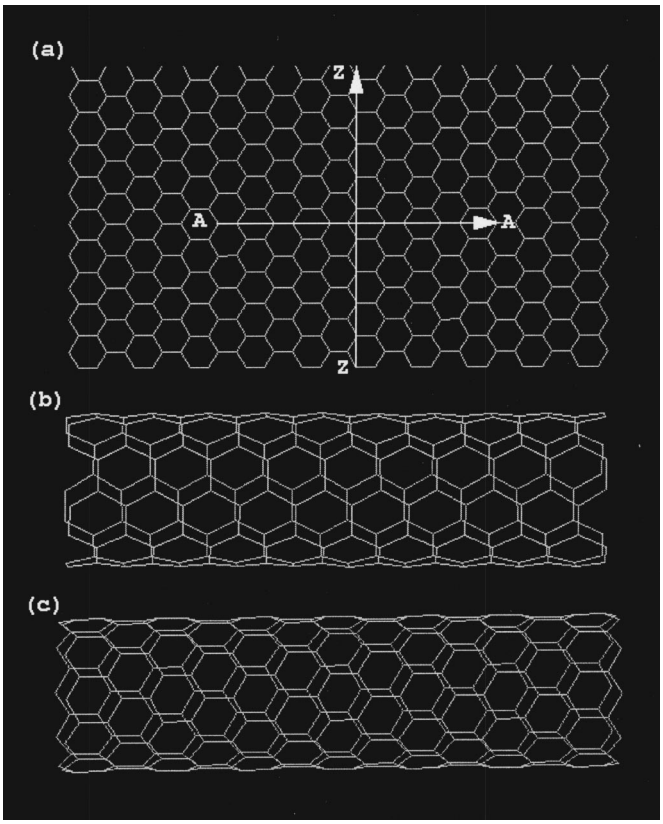

Fig. 1 *a*) A graphene sheet made of C atoms placed at the corners of hexagons forming the lattice with arrows AA and ZZ denoting the rolling direction of the sheet to make *b*) an (5,5) armchair and (c) a (10,0) zigzag nanotubes, respectively.

The single- and multi-wall nanotubes are interesting nanoscale materials for the following four reasons:

1) Single- and multi-wall nanotubes have very good elastic-mechanical properties because the two-dimensional (2D) arrangement of carbon atoms in a graphene sheet allows large out-of-plane distortions, while the strength of carbon-carbon in-plane bonds keeps the graphene sheet exceptionally strong against any in-plane distortion or fracture. These structural and material characteristics of nanotubes point towards their possible use in making next generation of extremely lightweight, but highly elastic, and very strong composite materials.
2) A single-wall nanotube can be either conducting or semiconducting, depending on its chiral vector (n, m), where n and m are two integers. The rule is that when the difference n-m is a multiple of three, a conducting nanotube is obtained. If the difference is not a multiple of three, a semiconducting nanotube is obtained. In addition, it is also possible to connect nanotubes with different chiralities creating nanotube hetero-junctions, which can form a variety of nanoscale molecular electronic device components.
3) Nanotubes, by structure, are high aspect-ratio objects with good electronic and mechanical properties. Consequently, the applications of nanotubes in field-emission displays or scanning probe microscopic tips for metrological purposes, have started to materialize even in the commercial sector.
4) Since nanotubes are hollow, tubular, caged molecules, they have been proposed as lightweight large surface area packing material for gas-storage and hydrocarbon fuel storage devices, and gas or liquid filtration devices, as well as nanoscale containers for molecular drug-delivery and casting structures for making nanowires and nanocapsulates.

A broad interest in nanotubes derives from the possibilities of a variety of applications in all of the above four technologically interesting areas. In this review, we mainly focus on the exceptionally stiff and strong mechanical properties that can be used for making future generation of lightweight structural composite materials. The other three interesting electrical, surface area, and aspect-ratio characteristics could be used to impart specific functional behavior to the thus prepared composite materials.

3 SIMULATION TECHNIQUES

In earlier days, the structural, mechanical, and thermal properties of interacting, bulk condensed matter systems were studied with analytical approximation methods for infinite systems. Numerical computer simulations of the finite sample systems have become more common recently because powerful computers to simulate nanoscale systems in full complexity are readily available. Atomistic molecular dynamics (MD) refers most commonly to the situation where the motion of atoms or molecules is treated in approximate finite difference equations of Newtonian mechanics. Except when dealing with very light atoms and very low temperatures, the use of the classical MD method is well justified. In MD simulation, the dynamic evolution of the system is governed by Newton's classical equation of motion, $d^2\mathbf{R_I}/dt^2 = \mathbf{F_I} = -dV/d\mathbf{R_I}$, which is derived from the classical Hamiltonian of the system, $H = \Sigma \mathbf{P_I^2}/2M_\mathbf{I} + V(\{\mathbf{R_I}\})$. The atomic forces are derived as analytic derivatives of the interaction energy functions, $\mathbf{F_I}(\{\mathbf{R_I}\}) = -dV/d\mathbf{R_I}$, and are used to construct Newton's classical equations of motion which are second-order ordinary differential equations. In its global structure, a general MD code typically implements an algorithm to find a numerical solution of a set of coupled first-order ordinary differential equations given by the Hamiltonian formulation of Newton's second law [6]. The equations of motion are numerically integrated forward in finite time steps using a predictor-corrector method.

The MD code for carbon based systems involves analytic many-body force field functions such as Tersoff-Brenner [7] potentials for C-C and C-H interactions [8]. The Tersoff-Brenner potential is specially suited for carbon-based systems, such as diamond, graphite, fullerenes, and nanotubes, and has been used in a wide variety of scenarios with results in agreement with experimental observations. Currently, there is no universal analytic many-body force field function that works for all materials and in all scenarios. A major distinguishing feature of the Tersoff-Brenner potential for carbon-based systems is that short-range bonded interactions are reactive, so that chemical bonds can form and break during the course of a simulation. Therefore, compared to some other molecular dynamics codes, the neighbor list describing the environment of each atom includes only a few atoms and needs to be updated more frequently. The computational cost of the many-body bonded interactions is relatively high compared to the cost of similar methods with non-reactive interactions with simpler functional forms. As a result, the overall computational costs of both short-range interactions and long-range, non-bonding van der Waals (Lennard-Jones 6–12) interactions are roughly comparable. For large-scale atomistic modeling (10^5–10^8 atoms), multiple processors are used for MD simulations, and the MD codes are generally parallelized [9].

In recent years, several more accurate quantum molecular dynamics schemes have been developed in which the forces between atoms are computed at each time step via quantum mechanical calculations within the Born-Oppenheimer approximation. The dynamic motions for ionic positions are still governed by Newtonian or Hamiltonian mechanics and described by molecular dynamics.

In the most general approach of full quantum mechanical description of materials, atoms are described as a collection of quantum mechanical particles, nuclei, and electrons, governed by the Schrödinger equation, $\boldsymbol{H}\Phi[\{\mathbf{R_I}, \mathbf{r}\}] = E_{tot}\Phi[\{\mathbf{R_I}, \mathbf{r}\}]$, with the full quantum many-body Hamiltonian operator $\boldsymbol{H} = \Sigma \mathbf{P_I^2}/2M_\mathbf{I} + \Sigma Z_I Z_J e^2/R_{IJ} + \Sigma \mathbf{p^2}/2m_\mathbf{e} + \Sigma e^2/r - \Sigma Z_I e^2/|\mathbf{R_I} - \mathbf{r}|$, where $\mathbf{R_I}$ and $\mathbf{r}$ are nuclei and electron coordinates. Using the Born-Oppenheimer approximation, the electronic degrees of freedom are assumed to follow adiabatically the corresponding nuclear positions, and the nuclei coordinates become classical variables. With this approximation, the full quantum many-body problem is reduced to a quantum many-electron problem $\boldsymbol{H}[\mathbf{R_I}]\Psi[\mathbf{r}] = E_{el}\Psi[\mathbf{r}]$, where $\boldsymbol{H} = \Sigma \mathbf{P_I^2}/2M_\mathbf{I} + \boldsymbol{H}[\mathbf{R_I}]$.

In the intermediate regimes, for up to few thousand atoms, the tight-binding [10] molecular dynamics (TBMD) approach provides very good accuracy for both structural and mechanical characteristics. The computational efficiency of the tight-binding method derives from the fact that the quantum Hamiltonian of the system can be parameterized. Furthermore, the electronic structure information can be easily extracted from the tight-binding Hamiltonian, which in addition also contains the effects of angular forces in a natural way. In a generalized *non-orthogonal* tight-binding molecular dynamics (TBMD) scheme, Menon and Subbaswami have used a minimal number of adjustable parameters to develop a transferable scheme applicable to clusters as well as bulk systems containing Si, C, B, N, and H [11,12]. The main advantage of this approach is that it can be used to find an energy-minimized structure of a nanoscale system under consideration without symmetry constraints.

Additionally, the *ab-initio* or first principles method is a simulation method to directly solve the complex quantum many-body Schrödinger equation using numerical algorithms [13]. An *ab-initio* method provides a more accurate description of quantum mechanical behavior of materials properties even though the system size is currently limited to only about few hundred atoms. Current *ab-initio* simulation methods are based on a rigorous mathematical foundation of the density functional theory (DFT) [14,15]. This is derived from the fact that the ground state total electronic energy is a functional of the density of the system. Kohn and Sham [14,15] have shown that the DFT can be reformulated as a single-electron problem with self-consistent effective potential, including all the exchange-correlation effects of electronics interactions:

$$\boldsymbol{H}_1 = \mathbf{p^2}/2m_\mathbf{e} + V_H(\mathbf{r}) + X_{XC}[\rho(\mathbf{r})] + V_{ion\text{-}el}(\mathbf{r}),$$

$$\boldsymbol{H}_1\psi(\mathbf{r}) = \varepsilon\psi(\mathbf{r}), \quad \text{for all atoms}$$

$$\rho(\mathbf{r}) = \Sigma|\psi(\mathbf{r})|^2.$$

This single-electron Schrödinger equation is known as the Kohn-Sham equation, and the local density approximation

(LDA) has been introduced to approximate the unknown effective exchange-correlation potential. This DFT-LDA method has been very successful in predicting materials properties without using any experimental inputs other than the identity of the constituent atoms.

For practical applications, the DFT-LDA method has been implemented with a pseudopotential approximation and a plane wave (PW) basis expansion of single-electron wave functions [13]. These approximations reduce the electronic structure problem to a self-consistent matrix diagonalization problem. One of the popular DFT simulation programs is the Vienna Ab intio Simulation Package (VASP), which is available through a license agreement (VASP) [16].

The three simulation methods described above each have their own advantages and are suitable for studies for a variety of properties of material systems. MD simulations have the least computational cost, followed by Tight Bending methods. Ab initio methods are the most costly among the three. MD simulations can study systems with up to millions of atoms. With well-fitted empirical potentials, MD simulations are quite suitable for studies of dynamical properties of large-scale systems, where the detailed electronic properties of systems are not always necessary. While DFT methods can provide highly accurate, self-consistent electronic structures, the high computational cost limits them to systems up to hundreds of atoms currently. To take the full capacity of DFT methods, a careful choice of an appropriate sized system is recommended. Tight Binding methods lay in between MD simulations and DFT methods, as to the computational cost and accuracy, and are applicable for systems up to thousands of atoms. For moderate-sized systems, TB methods can provide quite accurate mechanical and electronic characteristics.

For computational nanomechanics of nanotubes, all three simulation methods can be used in a complementary manner to improve the computational accuracy and efficiency. Based on experimental observations or theoretical dynamic and structure simulations, the atomic structure of a nanosystem can first be investigated. After the nanoscale system configurations have been finalized, the functional behaviors of the system are investigated through static *ab-initio* electronic energy minimization schemes. We have covered this in detail in a recent review article focusing exclusively on computational nanotechnology [17].

In the following, we describe nanomechanics of nanotubes and nanotube-polymer composites, and compare the simulation results, where ever possible, with experimental observations.

4 MODULUS OF NANOTUBES

The modulus of the nanotube is a measure of the stiffness against small axial stretching and compression strains, as well as non-axial bending and torsion strains on the nanotubes. The simulation results mainly pertain to the stiffness of SWNTs, where as most of the experimental observations available so far are either on MWNTs or ropes/bundles of nanotubes. For axial strains, SWNTs are expected to be stiffer than the MWNTs because of smaller radii of curvature and relatively defect free structure. For non-axial strains such as bending and torsion, the MWNTs are expected to be stiffer than the SWNTs. In this section, the axial, bending, and torsion moduli of SWNTs are described and compared with experimental observations known so far.

4.1 Young's modulus for axial deformations

As described above, single-wall carbon nanotubes have tubular structure that can be conceptualized by taking a graphene sheet, made of C atoms, and rolling into a long tubular shape. Contributions to the strength and stiffness of SWNTs come mainly from the strength of graphene in-plane covalent C—C bonds. It is expected that modulus, strength, and stiffness of SWNTs should be comparable to the in-plane modulus and strength of the graphene sheet. In the tubular shape, however, the elastic strain energies are affected by the intrinsic curvature of C—C bonds. Robertson *et al* [18] have found (using both Tersoff and Tersoff-Brenner potentials) that the elastic energy of a SWNT scales as $1/R^2$, where R is the radius of the tube. This is similar to the results deduced from continuum elastic theory [19]. The elastic energy of CNTs responding to a tensile stress in their study suggested that SWNTs are very strong materials and that the strength is mainly due to the strong C—C sp^2 bonds on the nanotube. The Young's modulus of a SWNT is $Y=(1/V)\partial^2 E/\partial\varepsilon^2$, where E is the strain energy and V is the volume of the nanotube.

Initial computational studies [20], using the same Tersoff-Brenner potential, reported the value of Young's modulus to be as high as 5.5TPa. This was mainly due to a very small value of wall thickness (h$\sim$0.06 nm) used in these studies. Using an empirical force constant model, Lu [21] found that the Young's modulus of a SWNT is approximately 970GPa, which is close to that of a graphite plane, and is independent of tube diameter and chirality. Rubio *et al* [22] used a better description for interatomic forces through a non-orthogonal tight-binding method and found the Young's modulus to be approximately 1.2TPa, which is larger than that of graphite, and is slightly dependent on the tube size especially for small diameter nanotubes (D$<$1.2 nm). High surface curvature for small diameter nanotubes tends to decrease the Young's modulus. The Young's modulus of a variety of carbon and also non-carbon nanotubes as a function of tube diameter in Rabio *et al*'s studies is shown in Fig. 2. In both Lu and Rabio *et al*'s studies, the thickness of the nanotube wall was assumed to be 0.34 nm (the van der Waals distances between graphite planes), and the computed modulus is within the range of experimental observations, as will be discussed below.

Later on, using the ab initio density functional theory (with pseudopotentials), Rubio *et al* [23] have found that the stiffness of SWNTs is close to that of the in-plane stiffness of graphite, and SWNTs made of carbon are strongest as compared with other non-carbon, such as boron-nitride (BN) or $B_xC_yN_z$, nanotubes known so far. The Young's modulus of Multi Wall CNTs (MWCNTs) and SWCNT ropes as a function of tube diameters from Rabio *et al*'s study is shown in Fig. 3.

Table 1. Summary of Young's modulus from various theoretical calculations used in different studies (where *Y* is Young's modulus and *h* is the wall thickness)

Method	Molecular dynamics Tersoff-Brenner force field [20]	Empirical force constant model [21]	Non-orthogonal tight-binding [22]	Ab initio DFT [23]
h	0.06 nm	0.34 nm	0.34 nm	0.34 nm
Y	SWCNT: 5.5 TPa	SWCNT: 0.97 TPa	SWCNT: 1.2 TPa	SWCNT rope: 0.8 TPa; MWCNT: 0.95 TPa

Table 2. Summary of Young's modulus from various experimental studies (with definitions of *Y* and *h* same as in Table 1)

Method	Thermal vibrations [28]	Restoring force of bending [29]	Thermalvibrations [30]	Deflection forces [31]
h	0.34 nm	0.34 nm	0.34 nm	0.34 nm
Y	MWCNT: 1.8 ± 1.4 TPa	MWCNT: 1.28 ± 0.59 TPa	SWCNT: 1.7 TPa	SWCNT: 1.0 TPa

The calculated Young's modulus from the above various methods is summarized in Table 1. The different results from various theoretical studies arise from the use of different definitions of carbon nanotube wall thickness, or different atomic interaction potentials. It has been suggested that by investigating the value $\partial^2 E/\partial \varepsilon^2$ instead of Young's modulus, the ambiguity of thickness of the CNT wall can be avoided.

Using a non-orthogonal tight-binding molecular dynamics method and the DFT method, we recently carried out [24] axial compression of single-wall C and BN nanotubes and have found Young's modulus to be about 1.2TPa, we also found that the modulus of a similar BN nanotube is about 80% of that of the carbon nanotube. These results are in qualitative and quantitative agreement with Rubio's DFT results and the general experimental observations known so far.

There have been attempts to use continuum theory to describe the elastic properties of carbon nanotubes. The value of the wall thickness of CNTs is usually required when applying a continuum elastic model, and it is not immediately clear how to define wall-thickness for systems where only a single layer of atoms form the wall. There are suggestions to use the value of $\partial^2 E/\partial \varepsilon^2$ instead of Young's modulus to avoid the ambiguity in the definition of wall thickness of nanotubes. Some recent studies by Ru [25] also use an independent variable as bending stiffness for nanotubes and avoid the parameter corresponding to the wall thickness altogether. However, in the description of continuum theory based models, the definition of wall thickness is important and needs to be consistent with the experimental results as well as those obtained from atomistic or tight-binding molecular dynamics simulations. According to Tables 1 and 2, the value of 0.34 nm for the wall thickness of a single-wall carbon nanotube gives experimental and atomistic simulation based results of Young's modulus that are in broad agreement with each other. This means that 0.34 nm, corresponding to the van der Waal radius of a single C atom, is a

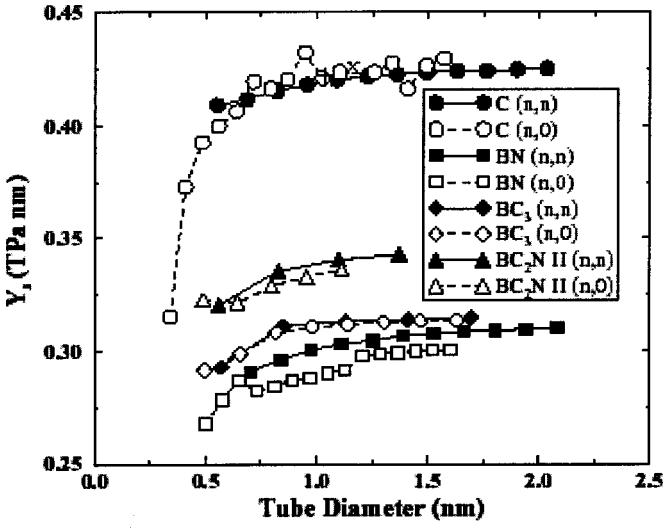

Fig. 2 Young's modulus as a function of the tube diameter for C, BN, BC3, BC2N from tight binding simulation [22].

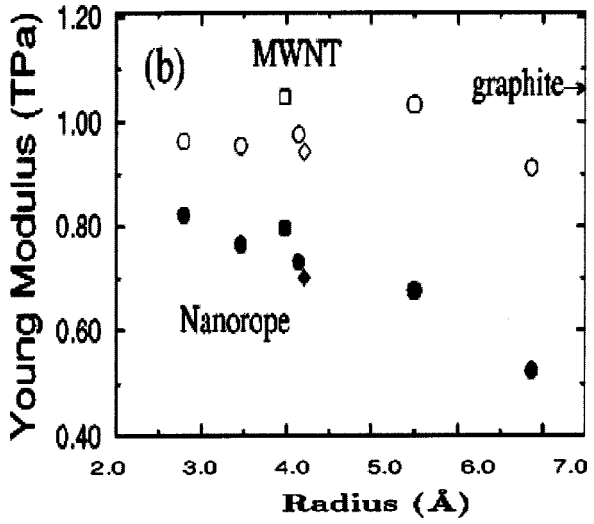

Fig. 3 Young's modulus verse tube diameter for ab initio simulation. Open symbols for the multiwall CNT geometry and solid symbols for the single wall tube with crystalline-rope configuration. The experimental value of the elastic modulus of graphite is also shown [23].

reasonable assumption for the wall thickness for evaluation of Young's modulus. A recent work by Harik [26] examines the validity of using continuum elastic theory for nanotubes and suggests that small and large diameter nanotubes need to be described with different approaches, such as a solid rod model for small diameter nanotubes and a shell model for large diameter nanotubes. This is also consistent with using 0.34 nm for wall thickness, because thin nanotubes with about 0.7 nm diameter would behave as a solid rod and not as a cylindrical shell, as was assumed earlier.

4.2 Bending stiffness and modulus

Besides axial strains discussed above, SWNTs have also been subjected to bending and torsional strains. The bending stiffness of a SWNT is $(1/L)d^2E/dC^2$, where E is the total strain energy, L is the length, and C is the curvature of the bent nanotube, which is related with the bending angle θ as $C=\theta/L$. From the elastic theory of bending of beams, the strain energy of a bent nanotube can be expressed as $E=0.5YhL\oint t^2C^2dl$, where Y is the Young's modulus of the SWNT, and h is the thickness of the wall [27]. The integral is taken around the circumference of the nanotube, and t is the distance of atoms from the central line (or the bent axis) of the tube. From this expression, the bending stiffness K is found to be equal to $Yh(\pi r^3)$, and scales as the cube of the radius of the tube. Results from molecular dynamics simulations with the Tersoff-Brenner potential show that the stiffness K scales as $R^{2.93}$ (Fig. 4), which is in good agreement with scaling predicted by the continuum elastic theory. The corresponding bending Young's modulus (Y_B) of SWNTs with varied diameters can be calculated from the above equation. For a small diameter SWNT Y_B is found to be about 0.9 TPa, smaller than the stretching Young's modulus calculated from the tight-binding method or first principle theory. The computed smaller value is also similar to what Robertson *et al* [18] showed in their study of the elastic energy of SWNTs. The qualitative agreement is rather good. An additional feature is that the bending Young's modulus decreases with the increase in tube diameter. This is mainly due to more favorable out-of-plane displacements of carbon atoms on a larger diameter tube, resulting in flattening of the tube in the middle section.

Poncharal *et al* [28] experimentally studied the bending Young's modulus of MWNTs (diameter>10 nm) using electrically induced force and have found that the bending Young's modulus is decreased sharply with the increase in tube diameter (Fig. 5*a*), which they have attributed to the wave-like distortion of the MWNT, as shown in Fig. 5*b*.

At a large bending angle, SWNTs can buckle sideways

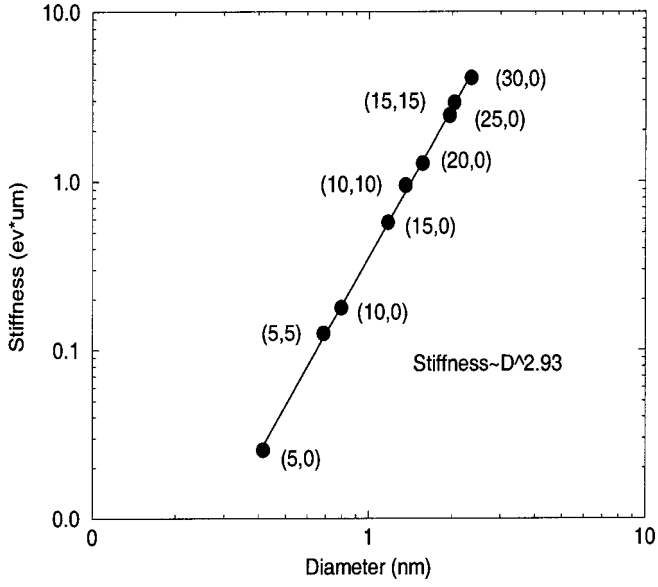

Fig. 4 Bending stiffness as a function of tube diameter from MD simulation with Tersoff-Brenner potential. The stiffness is scaled as $D^{2.93}$, closed to the cubic dependence on diameter D predicted from continuum elastic theory.

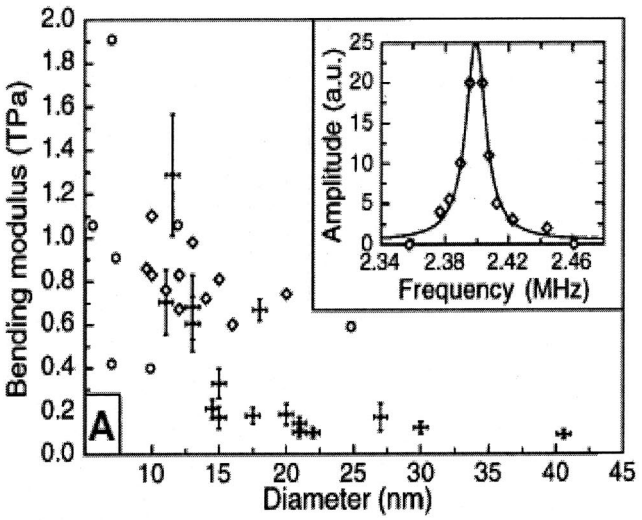

(*a*)

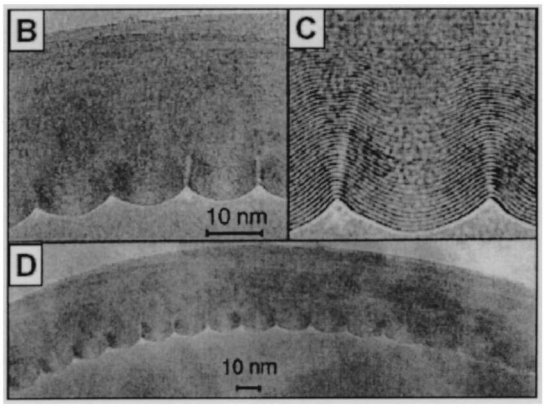

(*b*)

Fig. 5 *a*) Bending modulus as a function of tube diameter. Solid circles are from Poncharal *et al* [28]; others are from other experiments as referred in Poncharal *et al*'s paper. The dropping in the bending modulus is attributed to the onset of a wavelike distortion in lateral direction as shown in *b*). *b*) High–resolution TEM image of a bent nanotube (Radius of curvature ≈400 nm), showing the wavelike distortion and the magnified views [28].

similarly to a macroscopic rod, at which non-uniform strain is induced. Shown in Fig. 6*a* and *b* are the images from a high-resolution electron microscope [29] of the buckling of bent SWNT and MWCNT. Such buckling at large bending angle is closely related with buckling of a SWNT under axial compression stress, which will be discussed later.

4.3 Torsion stiffness and modulus

The torsion stiffness of a CNT is $K=(1/L)d^2E/d\theta^2$, where E is the total strain energy and θ is the torsion angle. The shear strain is related with torsion angle as $\varepsilon=R\theta/L$, where R is the radius of tube, and L is its length. From continuum elastic theory, the total strain energy of a cylinder can be written as $E=\frac{1}{2}G\int\int\int\varepsilon^2 dV$, where G is shear modulus of the tube. The torsion stiffness thus is related with G as $K=(1/L)d^2E/d\theta^2=G(2\pi h)R^3/L^2$, where h is the thickness of the wall of the nanotube. In Fig. 7, we show our recently computed values of the torsion stiffness of several armchair and zigzag carbon nanotubes using the Tersoff-Brenner potential. The dependence of the torsion stiffness on the radius of tube is found to be as $K\propto R^{3.01}$ (for tube diameter >0.8 nm). This is in excellent agreement with the prediction of cubic dependence from the continuum elastic theory.

The shear modulus of CNTs is found to be around 0.3 TPa and is not strongly dependent on diameters (for $D>0.8$ nm). This value is smaller than that of about 0.45 TPa in Lu's study [20], calculated with an empirical force constant model. For small diameter tubes, such as a (5,5) nanotube, the shear modulus deviates away from the continuum elastic theory description.

4.4 Experimental status: Modulus of carbon nanotubes

The high stiffness of carbon nanotubes has been verified by several experiments. Treacy *et al* [30] studied Young's modulus of MWNTs by measuring the thermal vibrations, and Y was found to be about (1.8 ± 1.4) TPa. Later research by Wong *et al* [31] on MWCNT found the Young's modulus to be about (1.28 ± 0.59) TPa by measuring the restoring force of bent nanotubes. Krishnan *et al* [32] conducted a study on the stiffness of single-walled nanotubes and have found the average Young's modulus to be approximately 1.25 TPa. This is close to the experimental results obtained by Salvetat *et al* [33], where Y was found to be about 1 TPa. The measured Young's modulus from these various methods is summarized in Table 2.

5 PLASTIC DEFORMATION AND YIELDING OF NANOTUBES

Nanotubes under large strain go through two kinds of structural changes. First, early simulations by Yakobson *et al* [20] showed that under axial compression, nanotubes exhibit structural instabilities resulting in sideways buckling, but the deformed structure remains within the elastic limit. Second, under large strains, bonding rearrangements or transitions occur giving rise to permanent damage, plastic deformation, or yielding of nanotubes. In this section, we discuss the plastic deformation and failure of nanotubes under large axial compression and tensile strains. Critical dependence of the yielding of nanotubes on the applied strain-rate and the kinetic temperature of the simulation are also discussed through a model that shows that nanotubes may typically yield within 5–10% tensile strain at room temperature. This finding is in good agreement with the experimental observations on the breaking and yielding of MWNTs and the ropes or bundles of SWNTs.

5.1 Plastic deformation under compressive strain

Yakobson *et al* [20] found that SWNTs form non-uniform fin-like structures under large compressive strain (Fig. 8). The sideways displacement or buckling of tubes occurs, for larger strain, and contributes towards the relief of strain energy from the fin-like structures, but the tubes remain superelastic for more than 20% compressive strains. Experiments have observed a sideways buckling feature in compressed multi-wall nanotubes in polymer composite materials [34]. Another mode of plastic deformation of compressed thin nanotubes is also observed in the same experiments [34]; ie, the tubes remain essentially straight, but the structure collapses locally as shown in Fig. 9.

Srivastava *et al* [35] used a tight-binding molecular dynamics method and have found that within the Euler buckling length limitation, an (8,0) carbon nanotube collapses locally at 12% compressive strain. The local plastic collapse is due to a graphitic (sp^2) to diamond-like (sp^3) bonding

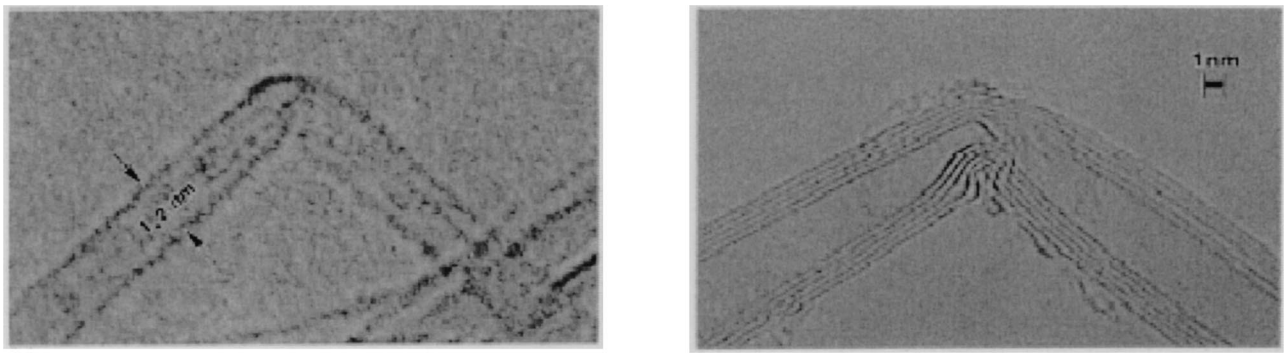

Fig. 6 HREM images of kink structures formed in bent CNTs. Shown on left is a single kink in a SWCNT with diameter 1.2nm; Shown on right is a kink on a MWCNT with diameter 8 nm [29].

transition at the location of the collapse and the release of excess strain in the remaining uncollapsed section. The released strain in the uncollapsed section drives the local collapse with a compressive pressure as high as 150 GPa at the location of the collapse (Fig. 10).

Srivastava *et al* [24] have also studied the influence of changes in the chemical nature on the nanomechanics and the plasticity of nanotubes. For example, this is done by considering the structure, stiffness, and plasticity of boron-nitride (BN) nanotubes. The results for Young's modulus of BN nanotubes have been discussed above. It turns out that BN nanotubes are only slightly less stiff (80–90%) as compared to their carbon equivalent. The tight-binding MD and

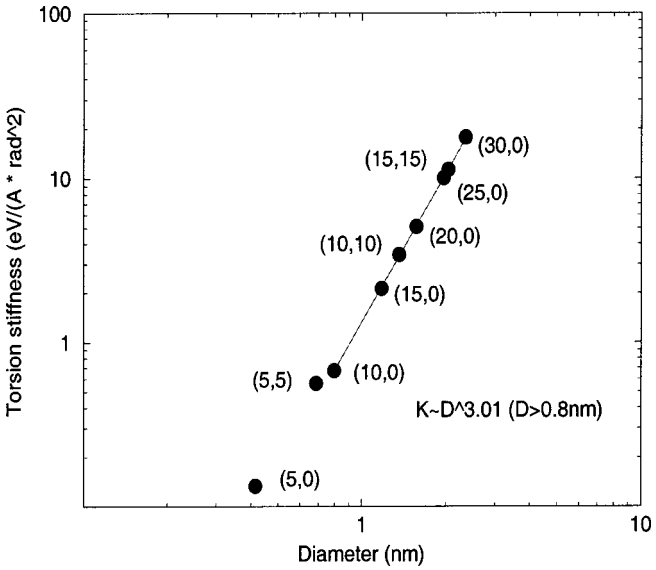

Fig. 7 The torsion stiffness as a function of tube diameter for a series of zigzag and armchair SWNTs calculated with Tersoff-Brenner potential. The stiffness is scaled as $D^{3.01}$ for D>0.8 nm, in agreement with the prediction from continuum elastic theory.

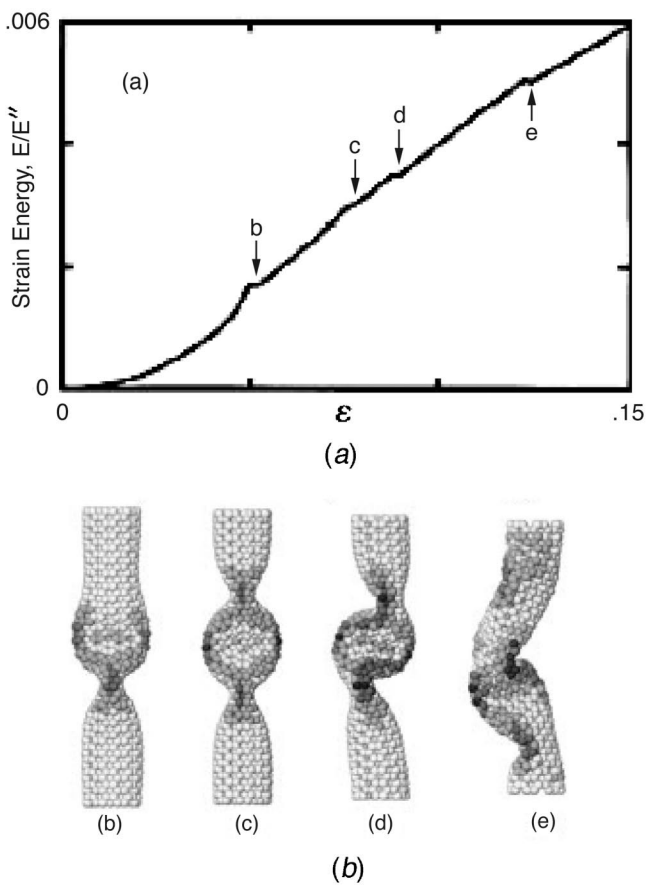

Fig. 8 *a*) The strain energy of a compressed 6 nm long (7,7) CNT, from Tersoff-Brenner potential, has four singularities corresponding to the buckled structures with shapes shown in *b* to *e*. The CNT is elastic up to 15% compression strain despite of the highly deformed structures. The MD study was conducted at T=0 K [20].

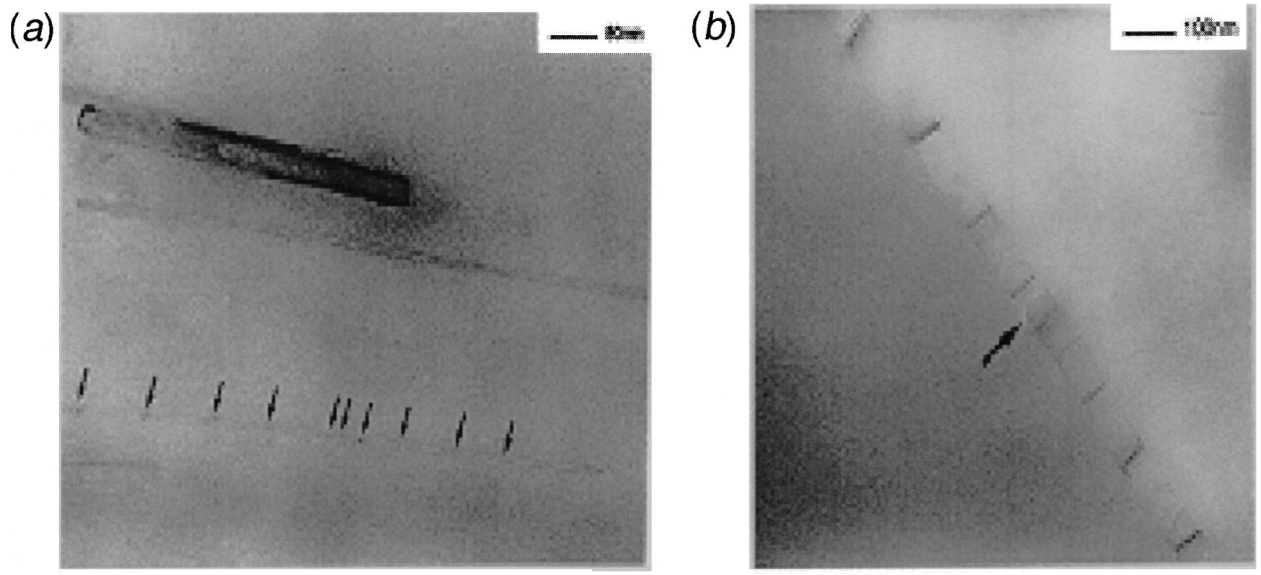

Fig. 9 TEM image of fractured multiwalled carbon nanotubes under compression within a polymeric film. The enlarged image is shown on right [52].

ab-initio total energy simulations further show that, due to BN bond rotation effect, BN nanotubes show anisotropic response to axial strains. For example, Fig. 11 shows spontaneous anisotropic plastic collapse of a BN nanotube that has been compressed at both ends, but strain release is shown to be more favorable towards nitride atoms in the rotated BN bonds. This results in the anisotropic buckling of the tube towards one end when uniformly compressed at both ends.

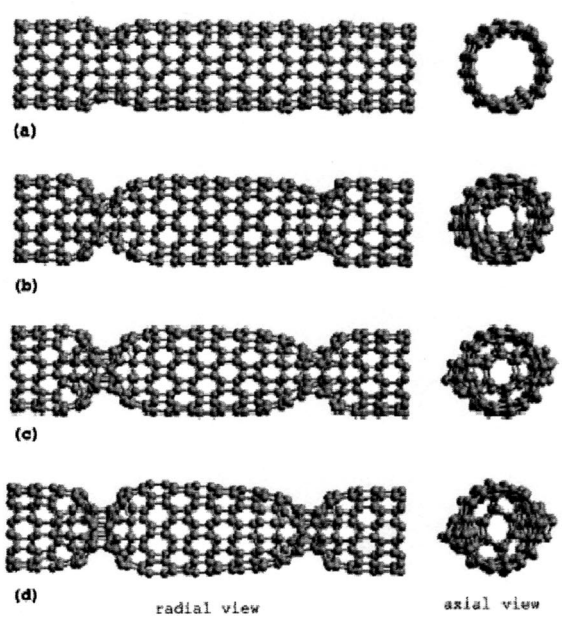

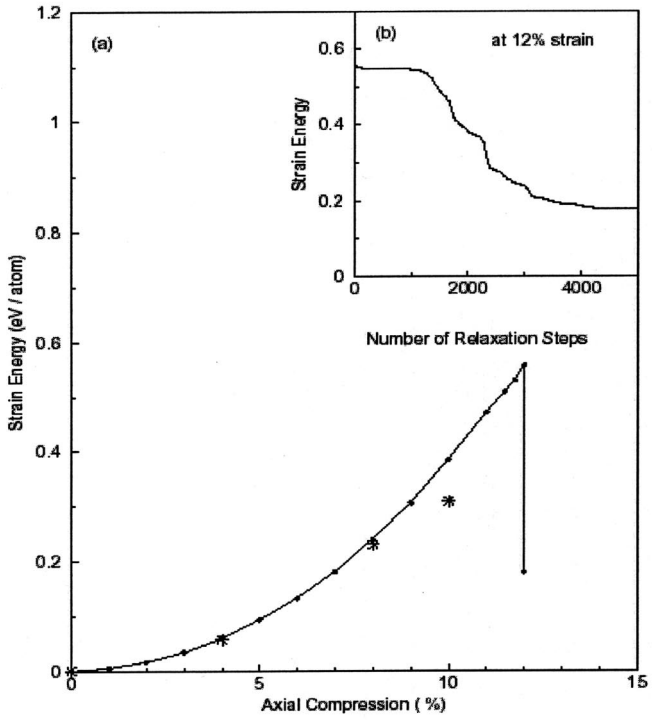

Fig. 10 Shown on top from *a* to *d* are four stages of spontaneous plastic collapse of the 12% compressed (8,0) CNT, with diamond like structures formed at the location of the collapse [35].

5.2 Plastic deformation under tensile strain

For the case of tensile strain, Nardelli *et al* [36,37] have studied the formation of Stone-Wales (SW) bond rotation induced defects as causing the plastic deformation of nanotubes. This mechanism is explained by formation of heptagon-pentagon pair (5775) defects in the walls of nanotubes (Fig. 12). The formation energy of such defects is decreased with the applied strain and is also dependent on the diameter and chirality of the nanotube under consideration. At high temperatures, plastic flow of the thus-formed defects occurs, and that can even change the chirality of the nano-

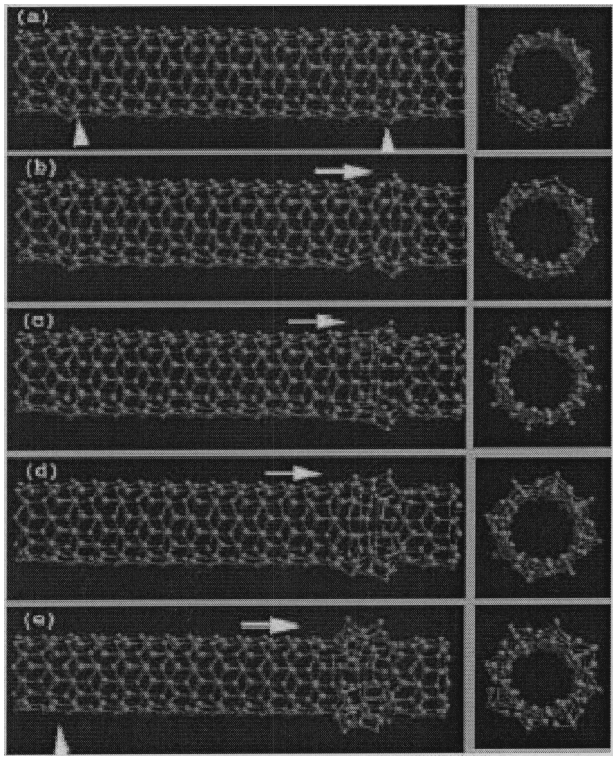

Fig. 11 Five stages of spontaneous plastic collapse of the 14.25% compressed (8,0) BN nanotube. *a*) Nucleation of deformations near the two ends, *b-d* anisotropic strain release in the central compressed section and plastic buckling near the right end of the tube, and *e*) the final anisotropically buckled structure where all the deformation is transferred toward the right end of the tube. The cross section of each structure is shown on right.

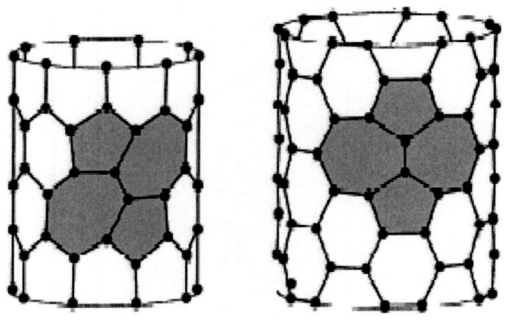

Fig. 12 The Stone Wales bond rotation on a zigzag and an armchair CNT, resulting pentagon-heptagon pairs, can lengthen a nanotube, with the greatest lengthening for an armchair tube [38].

tube (Fig. 13). On further stretch, the plastic flow and increased formations of more such defects continue until necking and breaking of the nanotube occurs. Zhang *et al* [38] have also examined the plastic deformations of SWNTs induced by the Stone-Wales dislocations under tensile strain, and they have found that the SW defects can release the strain energy in the system. Zhang *et al* note that SW defects form more favorably on an armchair nanotube than on a zigzag nanotube because the rotation of the C—C bond can compensate for more tensile strain along the axis in the former case.

5.3 Strain-rate and temperature dependence of yielding of nanotubes

In all the simulations and discussions so far, no dependence of the failure or yielding of nanotubes on the rate of the applied strain or the temperature of the system has been mentioned. This is because all of the above results were either obtained with the *ab-initio* or tight binding static total energy calculations or with MD simulations at much higher strain rates (than ever possible in experiments), where barriers to collapse would be *artificially* higher. In reality, it is expected that barrier to collapse and yielding strain at experimentally realizable strain rates and at room temperatures may be lower than the simulation values reported so far. The yielding or failure of SWNTs in different scenarios depends on the formation of defects discussed above. Classical MD simulations report values [39] as high as 30% yielding strain under tensile stretch and above 20% under compression [20]. Due to the limitations in the time scales of the phenomenon that can be simulated with MD, the nanotubes were typically strained at 1/ns at 300–600 K. The experiments so far suggest much lower yielding strains for nanotubes. Walters *et al* [40] have studied the SWNT rope under large tensile strain and observed the maximum strain to be $5.8\pm0.9\%$ before yielding occurs. Yu *et al* [41] have found similar breaking strain (5.3% or lower) for different SWNT rope samples (Fig. 14*a*). Similar measurements on MWNTs by Yu *et al* [42] show breaking strain to be about 12% or lower (the lowest one is 2% in their experiments) (Fig. 14*b*). The reported lower yielding strains in experiments could be partly due to tube defects in the SWNT ropes, or could be due to the much (orders of magnitude) lower rates at which strain can be applied in experiments.

The breaking, collapse, or yielding of the nanotubes are clearly a temperature and strain-rate-dependent phenomena, and a model needs to be developed to relate the reported much higher yielding strain from simulation studies to the so far observed lower yielding strain in experiments. Wei *et al* [43,44] have recently developed a transition-state theory based model for deducing strain rate and temperature dependence of the yielding strain as simulated in MD studies. According to the Arrhenius formula, the transition time for a system to go from the pre-yielding state to another (post yielding) state is dependent on the temperatures as $t=(1/\nu)e^{E_\nu/KT}$, where E_ν is the activation energy and ν is the effective vibration frequency or attempts for the transition. For a system with strain ε, the activation barrier is lowered as $E_\nu=E_\nu^0-kV\varepsilon$, where k is the force constant, and V is the activation volume. At higher temperatures, therefore, a system has larger kinetic energy to overcome the barrier

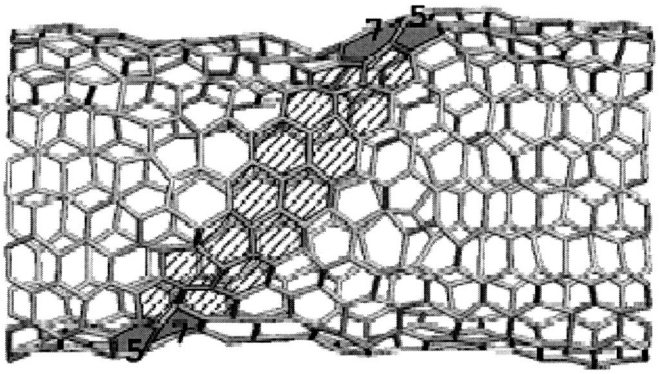

Fig. 13 A heptagon-pentagon pair appeared on a 10% tensile strain (10,10) CNT at T=2000 K. Plastic flow behavior of the Pentagon-heptagon pairs after 2.5ns at T=3000 K on a 3% tensile strained CNT. The shaded region indicates the migration path of the (5-7) edge dislocation [36].

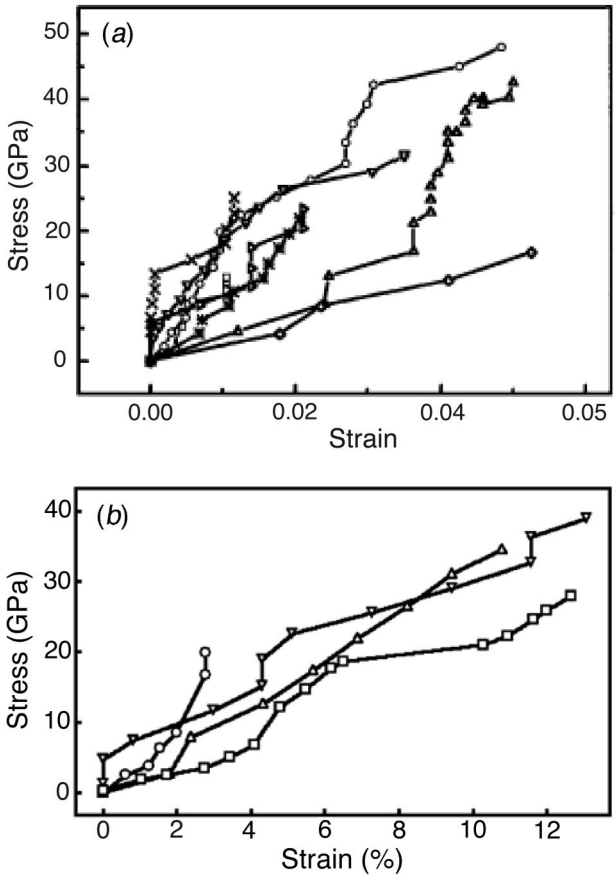

Fig. 14 Top: Eight stress versus strain curves obtained from the tensile-loading experiments on individual SWCNT ropes. The Young's modulus is ranged from 320GPa to 1470 GPa. The breaking strain was found at 5.3% or lower [41]. Bottom: Plot of stress versus strain curves for individual MWCNTs. The Young's modulus is ranged form 270GPa to 950 GPa, with breaking strain around 12% (one sample showed a 3% breaking strain) [42].

between the pre-yielding and post-yielding states, and the transition time is shortened. Similarly, the lower strain rate at each step allows the system to find an alternative minimum energy path, thus again lowering the effective barrier height separating the pre- and post-yielding states.

For example, yielding strain of a 6nm long (10,0) SWNT at several temperature and strain rate varying between $10^{-3}/ps$ to $10^{-5}/ps$, is shown in Fig. 15. Yielding strains are found to be 15% at low temperature and 5% at high temperature at about $10^{-5}/ps$ strain rate. Stone-Wales rotations are found to first appear before necking, resulting in heptagon and pentagon pairs, which provide the cores for formations of larger rings, and further resulting in the breakings of the nanotubes (Fig. 16). Detailed analysis [43,44] shows that the complex dependence on the temperature, and the strain rate with transition state theory (TST) can be expressed as $\varepsilon_Y = \overline{E}_\nu/YV + (KT/YV)\ln(N\dot{\varepsilon}/n_{site}\dot{\varepsilon}_0)$, where $\overline{E}_\nu$ is the averaged barrier for the yielding initiating defect, N is the number of processes involved in the breaking of the tube, Y is Young's modulus, n_{site} is the number of sites available for yielding, which is dependent on the structural details, and $\dot{\varepsilon}_0$ is a constant related to the vibration frequency of C—C bonds. For a more realistic strain rate such as 1%/hr, the yielding strain of the 6nm long (10,0) CNT can be estimated to be around 11%. A longer CNT will have a smaller yielding strain, as more sites are available for defects. The difference between the yielding strain of a nanometer long CNT and of a micron long CNT can be around 2% according to the above expression for the yielding strain [43,44]. The advantage of such a model is that one could directly compute the activation energy for yielding defect formation and get the yielding strain from the developed model. Within error bars on the known activation energies computed so far, our model is in very good agreement with experimental observations.

On the other hand, under compressive strain, as described above, Srivastava *et al* [35] showed that CNT collapses with the graphitic to diamond-like bonding transition at the location of the collapse. Another observation is the formation of non-uniform *fin*-like structures by Yakobson *et al* [20] that leads to sideways Euler buckling of the tube, and no diamond-like bonds or defects would form within the structure. Recent MD studies at finite temperatures [45] give different results. Using the same Tersoff-Brenner potential in MD studies, Wei *et al* [45] show that, with thermal activation, nanotubes under compressive strain can form both diamond-like bonds and SW-like dislocation defects at high temperatures (Fig. 17) [45]. Similar analysis of nanotubes under compressive strain therefore, is more complicated and

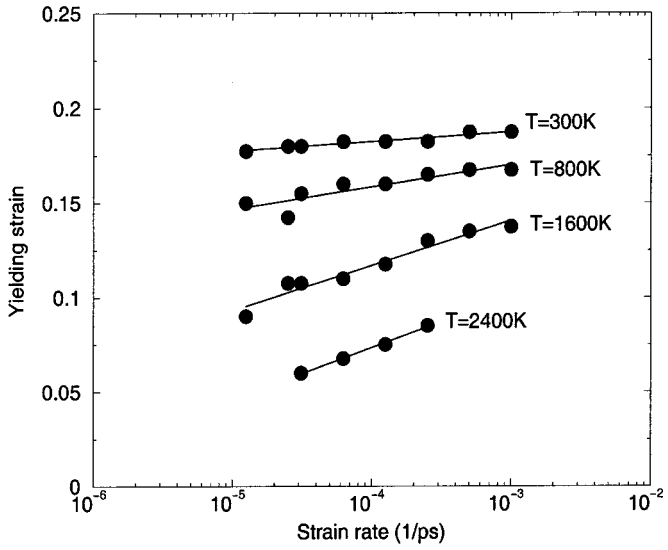

Fig. 15 The yielding strain of a 6nm long (10,0) CNT is plotted as functions of strain rate and temperature. Stone-Wales bond rotations appear first resulting in heptagon and pentagon ring; then larger C rings generated around such defects followed by the necking of the CNT; and the CNT is broken shortly after (from MD simulations with Tersoff-Brenner potential).

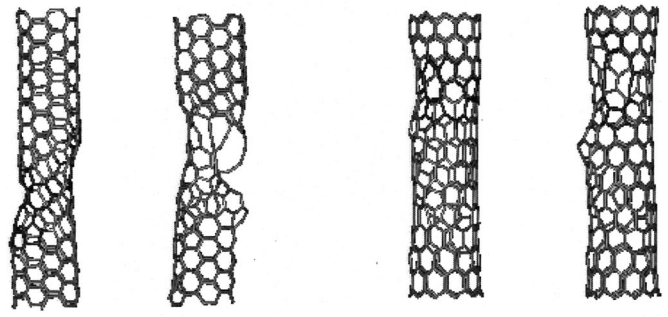

Fig. 16 Left: A 9% tensile strained (5,5) CNT with numerous Stone-Wales bond rotation defects at 2400K, and the following breaking of the tube. Right: An 11.5% tensile strained (10,0) with a group of pentagon and heptagon centered by an octagon at 1600K, and the following breaking of the tube (from MD simulation with Tersoff-Brenner potential).

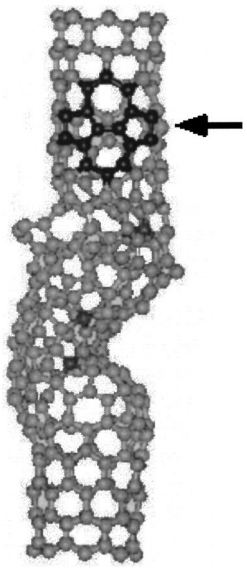

Fig. 17 A 12% compressed (10,0) CNT at T=1600 K. A Stone-Wales dislocation defect can be seen at the upper section of the CNT. Several sp3 bonds formed in the buckled region (from MD simulation with Tersoff-Brenner potential).

currently underway because sideways buckling can occur before tube yields with SW dislocation or diamond-like defect formation.

6 STRUCTURE AND MECHANICS OF NANOTUBE COMPOSITES

As discussed above, the strong in-plane graphitic C—C bonds make defect free SWNTs and MWNTs exceptionally strong and stiff against axial strains and very flexible against non-axial strains. Additionally, nanotubes also have very good electrical and thermal conduction capabilities. Many applications, therefore, are proposed for nanotubes as additive fibers in lightweight multi-functional composite materials. Several recent experiments on the preparation and characterization of nanotube-polymer composite materials have also appeared [46–48]. These measurements suggest modest enhancement in strength characteristics of CNT-embedded polymer matrices as compared to the bare polymer matrices. Vigolo *et al* [46] have been able to condense nanotubes in the flow of a polymer solution to form nanotube ribbons as well. These ribbons can be greatly bent without breaking and have Young's modulus that is an order of magnitude larger than that of the bucky paper. In the following, we discuss structural, thermal and mechanical implications of adding SWNTs to polyethylene polymer samples.

6.1 Structural and thermal behavior of nanotube-polyethylene composites

Thermal properties of polymeric materials are important from both processing and applications perspectives. As a function of temperature, polymeric materials go through structural transformation from solid to rubbery to liquid states. Many intermediate processing steps are done in the liquid or rubber-like state before the materials are cooled down to below glass transition temperature for the finally needed structural application. Besides the melting process at high temperature T_m, like other solid materials, the structural and dynamic behavior of polymeric material above and below glass transition temperature T_g is important to investigate. Below T_g the conformations of polymer chains are frozen, when polymers are in a solid glassy state, and in between T_g and T_m polymers are in a rubber-like state with viscous behavior. Preliminary experimental and simulation studies on the thermal properties of individual nanotubes show very high thermal conductivity of SWNTs [49]. It is expected, therefore, that nanotube reinforcement in polymeric materials may also significantly change the thermal and structural properties as well.

Atomistic MD simulation studies of the thermal and structural properties of a nanotube-polyethylene composites have been attempted recently [50]. Polyethylene is a linear chain molecule with CH_2 as the repeating unit in the chain. The density as a function of temperature for a pure polyethylene system (a short chain system with 10 repeating units in each polymer, with 50 polyethylene chains in the simulation sample) and a nanotube-polyethylene composite system with about 8% volume ratio capped nanotubes in the mixture is shown in Fig. 18. Both systems show discontinuity in the slope of the density-temperature curve. The discontinuities represent glass transition temperatures in the two cases. Two features are apparent in the figure. First, the glass transition temperature of the composite system has increased to a higher value than that of the pure polyethylene system. Second, above glass transition temperature in both the cases, the density as a function of temperature in the composite case decreases at a much faster rate than the decrease in the pure polyethylene system case. This means that the volume thermal expansion coefficient of the composite has increased to a larger value above glass transition temperature. The volume thermal expansion coefficient for the composite system above glass transition temperature is found to be $12 \times 10^{-4}\ \mathrm{K}^{-1}$, which is 40% larger than that of the pure polyethylene system above T_g. The increase in the thermal expansion coefficient due to mixing of SWNTs in the polymer sample is attributed to the increased excluded volume due to thermal motions of the nanotubes in the sample. In the same simulations, we also found that, above glass transition temperature, the self-diffusion coefficient of the polymer molecules in the composite increases as much as 30% above its pure polyethylene sample values. The increase in the diffusion coefficient is larger along the axis of the added nanotube fibers and could help during the processing steps due to better flow of the material above glass transition temperature.

6.2 Mechanical behavior of nanotube-polyethylene composites

Using fibers to improve the mechanical performance of a composite material is a very common practice, and the related technology has been commercialized for quite some time. Commonly used fibers are glass, carbon black, or other

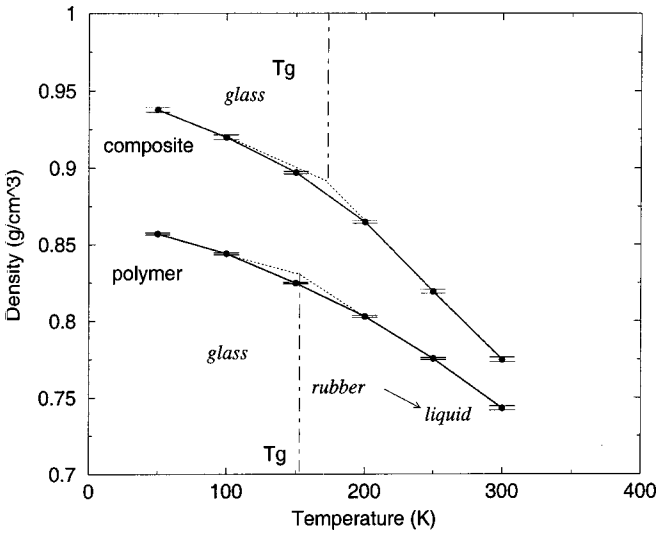

Fig. 18 Density as a function of temperature for a polyethylene system (50 chains with $Np=10$), and a CNT-polyethylene composite (2nm long capped (10,0) CNT) The CNT composite has an increase of thermal expansion above T_g. (From a MD simulation with Van der Waals potential between CNT and matrix. Dihedral angle potential and torsion potential were used for the polyethylene matrix, and Tersoff-Brenner potential was used for carbon atom on the CNT.)

ceramics. These not only can add structural strength to materials but also can add desired functionality in thermal and electrical behavior. The structural strength characteristics of such composite materials depend on the mechanical load transfer from the matrix to the fiber and the yielding of the coupling between the two. Mechanical load from matrix to the fibers in a composite is transferred through the coupling between the two. In some cases, the coupling is through chemical interfacial bonds, which can be covalent or noncovalent in nature, while in other one the coupling could be purely physical in nature through non-bonded van der Waals (VDW) interactions. Covalently coupled matrix and fibers are strongly interacting systems, while VDW coupled systems are weakly interacting systems, but occur in a wide variety of cases. The aspect ratio of fiber, which is defined as L/D (L is the length of the fiber, and D is the diameter), is also an important parameter for the efficiency of load transfers because the larger surface area of the fiber is better for larger load transfer. It is expected, therefore, that the embedded fibers would reach their maximum strength under tensile load only when the aspect ratio is large. The limiting value of the aspect ratio is found to be related to the interfacial shear stress τ as $L/D > \sigma_{\max}/2\tau$, where $\sigma_{\max}$ is the maximum strength of the fiber. Recent experiments on MWNTs or SWNT ropes [41,42] have reported the strength of the nanotubes to be in the range of 50GPa. With a typical value of 50MPa for the interfacial shear stress between the nanotube and the polymer matrix, the limiting value of the aspect ratio is 500:1. Therefore, for an optimum load transfer with a MWNT of 10nm diameter, the nanotube should be at least 5μm long, which is in the range of the length of nanotubes typically investigated in experiments on nanotube reinforced composites.

Earlier studies of the mechanical properties of the composites with macroscopic fibers are usually based on continuum media theory. Young's modulus of a composite is expected to be within a lower bound of $1/Y_{comp} = V_{fiber}/Y_{fiber} + V_{matrix}/Y_{matrix}$ and an upper bound of $Y_{comp} = V_{fiber}Y_{fiber} + V_{matrix}Y_{matrix}$, where V_{fiber} and V_{matrix} are the volume ratios of the fiber and the matrix, respectively. The upper bound obeys the linear mixing rule, which is followed when the fibers are continuous and the bonding between fibers and the matrix is perfect, ie, the embedded fibers are strained by the same amount as the matrix molecules. The lower bound is reached for the case of particulate filler composites because the aspect ratio is close to one. For a nanotube fiber composite, therefore, an upper limit can be reached if the nanotubes are long enough and the bonding with the matrix is perfect. Additionally, short nanotubes, with Poisson's ratio of about 0.1–0.2, are much harder material as compared to the polymer molecules with Poisson's ratio of about 0.44. Therefore, as a nanotube containing polymer matrix is stretched under tensile strain there is a resistance to the compression pressure perpendicularly to the axis of the tube. For the short, but hard nanotubes and soft polymer matrix mixture, this provides additional mechanism of load transfer that is not possible in other systems.

An MD simulation of the mechanical properties of a composite sample was recently performed with short nanotubes embedded in a short-chained polyethylene system at 50K, a temperature below glass transition temperature. The coupling at the interface was through non-bonded van der Waals interactions. Shown in Fig. 19 is the stress-strain curve for both the composite system and the pure polyethylene matrix system. Young's modulus of the composite is found to be 1900MPa, which is about 30% larger than that of the pure polymer matrix system. This enhancement is within the upper and lower bound limits discussed above. We have found that further enhancement of Young's modulus of the same sample can be achieved by carrying the system through repeated cycles of the loading-unloading of the tensile strain on the composite matrix. In agreement with the experimental observation, this tends to align the polymer molecules with the nanotube fibers, causing a better load transfer between the two. Frankland *et al* [51] have studied the load transfer between polymer matrix and SWNTs and have found that there was no permanent stress transfer for 100nm long (10,10) CNTs within polyethylene if only van der Waals interaction is present. In the study, they estimated that the interfacial stress could be 70MPa with chemical bonding between SWCNT and polymer matrix, while only 5MP for the nonbonding case.

6.3 Experimental status

Using nanotubes as reinforcing fibers in composite materials is still a developing field from theoretical and experimental perspectives. Several experiments regarding the mechanical properties of nanotube-polymer composite materials have been reported recently. Wagner *et al* [52] experimentally studied the fragmentation of MWNTs within thin polymeric films (urethane/diacrylate oligomer EBECRYL 4858) under compressive and tensile strain. They have found that nanotube-polymer interfacial shear stress τ is of the order of

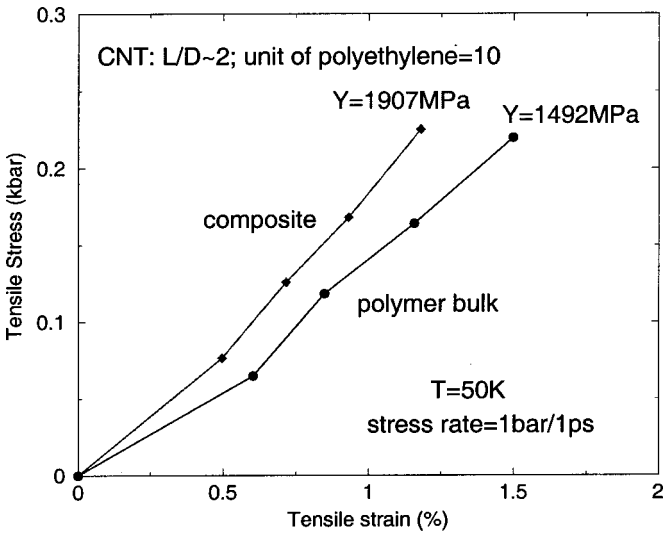

Fig. 19 Plot of the stress versus strain curve for pure polyethylene matrix and CNT composite (8 vol%) at small strain region (T = 50 K). Young's modulus is increased 30% for the composite (from MD simulation).

500MPa, which is much larger than that of conventional fibers with polymer matrix. This has suggested the possibility of chemical bonding between the nanotubes and the polymer in their composites. The nature of the bonding, however, is not clearly known. Later, Lourie *et al* [53] examined the fragmentation of single-walled CNT within the epoxy resin under tensile stress. Their experiment also suggested a good bonding between the nanotube and the polymer in the sample. Schadler *et al* [47] have studied the mechanical properties of 5% (by weight) MWNTs within epoxy matrix by measuring the Raman peak shift when the composites are under compression and under tension. A large Raman peak shift is observed for the case of compression, while the shift in the case of tension is not significant. The tensile modulus of the composites is found to enhance much less as compared to the enhancement in the compression modulus of the similar system. Schadler *et al* have attributed the differences, between the tensile and compression strain cases, to the sliding of inner shells of the MWNTs when a tensile stress is applied. In cases of SWNT polymer composites, the possible sliding of individual tubes in the SWCNT rope, which is bonded by van der Waals forces, may also reduce the efficiency of load transfer. It is suggested that for the SWNT rope case, interlocking using polymer molecules might bond the SWCNT rope more strongly. Andrews *et al* [48] have also studied composites of 5% (by weight) of SWNT embedded in petroleum pitch matrix, and their measurements show an enhancement of Young's modulus of the composite under tensile stress. Qian *et al*'s measurement of a 1% MWNT-polystyrene composite under tensile stress also shows a 36% increase of Young's modulus compared with the pure polymer system [54]. The possible sliding of inner shells in MWCT and of individual tubes in a SWNT rope was not discussed in these later two studies. There are, at present, no experiments available for SWNT-polymer composites to compare our simulated values with the experimental observations. However, if it is assumed that polymer matrix essentially bonds only to the outer shell of a MWNT embedded in a matrix, the above simulation findings could be qualitatively compared with experiments. This issue needs to be considered in more detail before any direct comparison is made between theory/simulations and experimental observations.

7 COMMENTS

Nanomechanics of single-wall carbon nanotubes have been discussed from a perspective of their applications in carbon nanotube reinforced composite materials. It is clear that for single-wall carbon nanotubes, a general convergence has started to emerge between the simulated Young's modulus values and the values observed in experiments so far. Young's modulus is slightly larger than 1TPa, and tubes can withstand about 5–10% axial strains before yielding, which corresponds to a stress of about 50 GPa before nanotubes yield. Bending and torsional modulus and stiffness have also been computed, but no comparison with experiments is available so far. Real progress is made in coming up with a transition state theory based model of the yielding of SWNTs under tensile stress. The yielding is identified as a barrier dependent transition between the pre- and post-yielding configurations. The model, within the error bars of the computed activation barrier, correctly predicts that under tensile strain at realistic (experimentally realizable) strain rates, yield occurs at about 5–10% applied strain, but not at high yielding strains of 20–30% as was predicted in the earlier MD simulations. Preliminary results of the structural, thermal, and mechanical characterization of nanotube polymer composites have been obtained and show that important characteristics such as thermal expansion and diffusion coefficients from the processing and applications perspective can be simulated for computational design of nanotube composite materials. These simulations illustrate the large potential of computational nanotechnology based investigations. For larger system sizes and realistic interface between nanotubes and polymer, the simulation techniques and underlying multi-scale simulations and modeling algorithms need to be developed and improved significantly before high fidelity simulations can be attempted in the near future.

ACKNOWLEDGMENTS

Part of this work (DS) was supported by NASA contract 704-40-32 to CSC at NASA's Ames Research center. KC and CW acknowledge a support from NASA contract NCC2-5400-2. KC acknowledges many helpful discussions with Dr M Baskes and Prof R Ruoff on nanotube mechanics.

REFERENCES

[1] Iijima S (1991), Helical microtubules of graphitic carbon, *Nature (London)* **354**, 56–58.
[2] Iijima S (1993), Single-shell carbon nanotubes of 1-nm diameter, *Nature (London)* **363**, 603–605.
[3] Bethune DS, Kiang CH, Devries MS, Gorman G, Savoy R, Vazquez J, and Beyers R (1993), Cobalt-catalyzed growth of carbon nanotubes with single-atomic-layerwalls, *Nature (London)* **363**, 605–607.
[4] Saito R, Dresselhaus G, and Dresselhaus MS (1998), *Physical Properties of Carbon Nanotubes*, Imperial College Press, London.
[5] Dresselhaus MS, Dresselhaus G, and Avouris Ph (eds) (2001), *Carbon Nanotubes: Synthesis, Structure, Properties, and Applications*, Springer-Verlag Berlin, Heidelberg.
[6] Allen MP and Tildsley DJ (1987), *Computer Simulations of Liquids*, Oxford Science Publications, Oxford.
[7] Brenner DW, Shenderova OA, and Areshkin DA (1998), *Reviews in Computational Chemistry*, KB Lipkowitz and DB Boyd (eds), 213, VCH Publishers, New York.
[8] Garrison BJ and Srivastava D (1995), Potential-energy surfaces for chemical-reactions at solid-surfaces, *Ann. Rev. Phys. Chem.* **46**, 373–394.
[9] Srivastava D and Barnard S (1997), Molecular dynamics simulation of large scale carbon nanotubes on a shared memory archi-tecture, *Proc. IEEE Supercomputing* **97** (SC'97 cd-rom), [Published]. [Paper No].
[10] Harrison WA (1980), *Electronic Structure and the Properties of Solids*, Freeman, San Francisco.
[11] Menon M and Subbaswamy KR (1997), Nonorthogonal tight-binding molecular dynamics scheme for silicon with improved transferability, *Phys. Rev. B* **55**, 9231–9234.
[12] Menon M (2001), Generalized tight-binding molecular dynamics scheme for heteroatomic systems: Application to SimCn clusters, *J. Chem. Phys.* **114**, 7731–7735.
[13] Payne MC, Teter MP, Allan DC, Arias TA, and Joannopoulos JD (1992), Iterative minimization techniques for abinitio total-energy calculations: molecular-dynamics and conjugate gradients, *Rev. Mod. Phys.* **68**, 1045–1097.
[14] Hohenberg P and Kohn W (1964), Inhomogeneous electron gas, *Phys. Rev. B* **136**, B864.
[15] Kohn W and Sham LJ (1965), Self-consistent equations including exchange and correlation effects, *Phys. Rev.* **140**, A1133.

[16] Check the web site for the details, http://cms.mpi.univie.ac.at/vasp/.
[17] Srivastava D, Menon M, and Cho K (2001), Computational nanotechnology with carbon nanotubes and fullerenes, (Special Issue on Nanotechnology) *Computing in Engineering and Sciences* **3**(4), 42–55.
[18] Robertson DH, Brenner DW, and Mintmire JW (1992), Energetics of nanoscale graphitic tubules, *Phys. Rev. B* **45**, 12592–12595.
[19] Tibbetts GG (1984), Why are carbon filaments tubular, *J. Cryst. Growth* **66**, 632–638.
[20] Yakobson BI, Brabec CJ, and Bernholc J (1996), Nanomechanics of carbon tubes: Instabilities beyond linear response, *Phys. Rev. Lett.* **76**, 2511–2514.
[21] Lu JP (1997), Elastic properties of carbon nanotubes and nanoropes, *Phys. Rev. Lett.* **79**, 1297–1300.
[22] Hernandez E, Goze C, Bernier P, and Rubio A (1998), Elastic properties of C and BxCyNz composite nanotubes, *Phys. Rev. Lett.* **80**, 4502–4505.
[23] Sanchez-Portal D, Artacho E, Solar JM, Rubio A, and Ordejon P (1999), Ab initio structural, elastic, and vibrational properties of carbon nanotubes, *Phys. Rev. B* **59**, 12678–12688.
[24] Srivastava D, Menon M, and Cho K (2001), Anisotropic nanomechanics of boron nitride nanotubes: Nanostructured ''skin'' effect, *Phys. Rev. B* **63**, 195413–195416.
[25] Ru CQ (2000), Effective bending stiffness of carbon nanotubes, *Phys. Rev. B* **62**, 9973–9976.
[26] Harik VM (2001), Ranges of applicability for the continuum beam model in the mechanics of carbon nanotubes and nanorods, *Solid State Commun.* **120**, 331–335.
[27] Landau LD and Lifschitz EM (1986), *Theory of Elasticity, 3rd Edition*, Pergamon Press, Oxford [Oxfordshire], New York.
[28] Poncharal P, Wang ZL, Ugarte D, and deHeer WA (1999), Electrostatic deflections and electromechanical resonances of carbon nanotubes, *Science* **283**, 1513–1516.
[29] Iijima S, Brabec C, Maiti A, and Bernholc J (1996), Structural flexibility of carbon nanotubes, *J. Chem. Phys.* **104**, 2089–2092.
[30] Treacy MMJ, Ebbesen TW, and Gibson JM (1996), Exceptionally high Young's modulus observed for individual carbon nanotubes, *Nature (London)* **381**, 678–680.
[31] Wong EW, Sheehan PE, and Lieber CM (1997), Nanobeam mechanics: Elasticity, strength, and toughness of nanorods and nanotubes, *Science* **277**, 1971–1975.
[32] Krishnan A, Dujardin E, Ebbesen TW, Yianilos PN, and Treacy MMJ (1998), Young's modulus of single-walled nanotubes, *Phys. Rev. B* **58**, 14013–14019.
[33] Salvetat JP, Briggs GAD, Bonard JM, Bacsa RR, Kulik AJ, Stockli T, Burnham NA, and Forro L (1999), Elastic and shear moduli of single-walled carbon nanotube ropes, *Phys. Rev. Lett.* **82**, 944–947.
[34] Lourie O, Cox DM, and Wagner HD (1998), Buckling and collapse of embedded carbon nanotubes, *Phys. Rev. Lett.* **81**, 1638–1641.
[35] Srivastava D, Menon M, and Cho K (1999), Nanoplasticity of single-wall carbon nanotubes under uniaxial compression, *Phys. Rev. Lett.* **83**, 2973–2676.
[36] Nardelli MB, Yakobson BI, and Bernholc J (1998), Brittle and ductile behavior in carbon nanotubes, *Phys. Rev. Lett.* **81**, 4656–4659.
[37] Nardelli MB, Yakobson BI, and Bernholc J (1998), Mechanism of strain release in carbon nanotubes *Phys. Rev. B* **57**, 4277–4280.
[38] Zhang PH, Lammert PE, and Crespi VH (1998), Plastic deformations of carbon nanotubes, *Phys. Rev. Lett.* **81**, 5346–5349.
[39] Yakobson BI, Campbell MP, Brabec CJ, and Bernholc J (1997), High strain rate fracture and C-chain unraveling in carbon nanotubes, *Comput. Mater. Sci.* **8**, 341–348.
[40] Walters DA, Ericson LM, Casavant MJ, Liu J, Colbert DT, Smith KA, and Smalley RE (1999), Elastic strain of freely suspended single-wall carbon nanotube ropes, *Appl. Phys. Lett.* **74**, 3803–3805.
[41] Yu MF, Files BS, Arepalli S, and Ruoff RS (2000), Tensile loading of ropes of single wall carbon nanotubes and their mechanical properties, *Phys. Rev. Lett.* **84**, 5552–5555.
[42] Yu MF, Lourie O, Dyer MJ, Moloni K, Kelly TF, and Ruoff RS (2000), Strength and breaking mechanism of multiwalled carbon nanotubes under tensile load, *Science* **287**, 637–640.
[43] Wei CY, Cho K, and Srivastava D (2002), Tensile strength of carbon nanotubes under realistic temperature and strain rate, http://xxx.lanl.gov/abs/condmat/0202513.
[44] Wei C, Cho K, and Srivastava D (2001), Temperature and strain-rate dependent plastic deformation of carbon nanotube, *MRS Symp Proc* **677**, AA6.5.
[45] Wei CY, Srivastava D, and Cho K (2002), Molecular dynamics study of temperature dependent plastic collapse of carbon nanotubes under axial compression, *Computer Modeling in Engineering and Sciences* **3**, 255–261.
[46] Vigolo B, Penicaud A, Coulon C, Sauder C, Pailler R, Journet C, Bernier P, and Poulin P (2000), Macroscopic fibers and ribbons of oriented carbon nanotubes, *Science* **290**, 1331–1334.
[47] Schadler LS, Giannaris SC, and Ajayan PM (1998), Load transfer in carbon nanotube epoxy composites, *Appl. Phys. Lett.* **73**, 3842–3844.
[48] Andrews R, Jacques D, Rao AM, Rantell T, Derbyshire F, Chen Y, Chen J, and Haddon RC (1999), Nanotube composite carbon fibers, *Appl. Phys. Lett.* **75**, 1329–1331.
[49] Osman MA, and Srivastava D (2001), Temperature dependence of the thermal conductivity of single-wall carbon nanotubes, *Nanotechnology* **12**, 21–24.
[50] Wei CY, Srivastava D, and Cho K (2002), Thermal expansion and diffusion coefficients of carbon nanotube-polymer composites, *Nano Lett.* **2**, 647–650.
[51] Frankland SJV, Caglar A, Brenner DW, and Griebe M (2000, Fall), Reinforcement mechanisms in polymer nanotube composites: simulated non-bonded and cross-linked systems *MRS Symp Proc*, **A14**.17.
[52] Wagner HD, Lourie O, Feldman Y, and Tenne R (1998), Stress-induced fragmentation of multiwall carbon nanotubes in a polymer matrix, *Appl. Phys. Lett.* **72**, 188–190.
[53] Lourier O, and Wagner HD (1998), Transmission electron microscopy observations of fracture of single-wall carbon nanotubes under axial tension, *Appl. Phys. Lett.* **73**, 3527–3529.
[54] Qian Q, Dickey EC, Andrews R, and Rantell T (2000), Load transfer and deformation mechanisms in carbon nanotube-polystyrene composites, *Appl. Phys. Lett.* **76**, 2868–2870.

Deepak Srivastava *is a senior scientist and technical leader of computational nanotechnology investigations at NASA Ames Research Center. In recent years, he has given about 100 presentations on carbon nanotubes and nanotechnology. His accomplishments include co-winner of Feynman Prize (Theory) in 1997, NASA Ames Contractor Council Award (1998), two Veridian Medal Paper Authorship awards (1999), NASA Group Excellence Award to IPT (2000), and The Eric Reissener Medal (2002) for distinguished contributions to nanoscience and carbon nanotubes. Srivastava serves as associate editor of two nanotechnology and computer modeling related peer reviewed journals, and sits on the advisory board of New York based Nano-Business Alliance.*

Chenyu Wei *is a research scientist at NASA Ames Research Center since 2002. She received a PhD in physics from the University of Pennsylvania in 1999 and worked as a postdoctoral fellow in the Laboratory for Advanced Materials and Department of Mechanical Engineering at Stanford University from 2000-2002. Her research area is in nanoscience, including mechanical and electronic properties of nanotubes and their composites, nanotube-polymer interfaces, and biomaterials.*

Kyepongjae (KJ) Cho *is an Assistant Professor of Mechanical Engineering and, by courtesy, in Materials Science and Engineering at Stanford University (1997-present). He received his PhD in Physics at MIT in 1994. During 1994-1997, he worked as a research staff member at the MIT Research Laboratory of Electronics and Harvard University. His research area is computational materials modeling using high-performance supercomputers. To investigate complex materials properties with true predictive power, his group is applying efficient atomistic simulation programs, which enable one to study increasingly larger complex materials systems with more accuracy. The complex materials systems he has studied using the atomistic method encompass a wide range of different chemical systems, biomolecules, and electronic materials.*